02

Optimization of chemical composition and structure of the photocatalyst of $ZnO-SnO_2-Fe_2O_3$ system

© D.A. Gavrilova[1,2], M.A. Gavrilova[1,2], L.L. Khomutinnikova[1], S.K. Evstropiev[1,2,3], I.K. Meshkovskii[1]

[1] ITMO University,
197101 St. Petersburg, Russia
[2] St. Petersburg State Institute of Technology (Technical University),
190013 St. Petersburg, Russia
[3] Vavilov State Optical Institute,
192171 St. Petersburg, Russia

e-mail: amonobel@yandex.ru

Received February 10, 2024
Revised March 10, 2024
Accepted April 07, 2024

The work carried out studies to optimize the chemical composition and structure of the photocatalyst of the $ZnO-SnO_2-Fe_2O_3$ system for sensor and medical applications. Photocatalytic materials were synthesized by liquid polymer-salt method and their structure and chemical composition were studied by XRD and SEM analysis and optical and luminescence spectroscopy. Obtained composites are composed from hexagonal ZnO crystals, tetragonal SnO_2 crystals and $ZnSn_2O_4$ spinel. The band gap values of prepared materials are 3.17–3.24 eV. The kinetic dependencies of the adsorption of organic diazo dye Chicago Sky Blue from solutions on the composite surfaces are successfully described by kinetic equations of as pseudo-first so as pseudo-second orders. The kinetics of photocatalytic dye decomposition under UV and visible irradiations is successfully described by kinetic equation of pseudo-first order. It was found that Ag addition allows to remarkably enhance adsorptive and photocatalytic properties of $SnO-SnO_2-Fe_2O_3$ materials.

Keywords: nanocrystals, heterostructure, photocatalysis, adsorption.

DOI: 10.61011/EOS.2024.04.58882.6016-24

Introduction

Photocatalytic materials for various practical applications (solar and hydrogen power engineering, medicine, photocatalytic installations for air and water purification and disinfection, etc.) are currently being developed actively.

The generation of reactive oxygen species (ROSs) by a photocatalyst under the influence of light and their interaction with the environment is the crucial mechanism of photocatalytic processes [1–4]. The ROS photogeneration intensity depends both on the parameters of excitation radiation and on the chemical composition, structure, and morphology of the photocatalytic material [5,6].

Processes of adsorption of organic compounds on the surface of photocatalysts play an important role in photocatalysis and have been the focus of a number of studies [5–9]. The adsorption of organic compounds on the surface of a photocatalyst was regarded in [9] as the first stage of a series of processes occurring during their photocatalytic decomposition.

One of the most common areas of application of photocatalytic processes is the purification of water from various harmful organic compounds and its disinfection from pathogenic microorganisms. Therefore, the rate of photocatalytic decomposition of an organic dye in an aqueous solution is often used as a criterion for assessing the efficiency of a photocatalyst.

It was demonstrated in numerous studies that the kinetics of decomposition of organic compounds with the aid of various photocatalysts is characterized adequately in most cases by a pseudo-first-order kinetic equation [6,8,9]. This allows one to use the rate constant of decomposition of an organic compound as a criterion for assessing the efficiency of photocatalysts in experiments performed under similar conditions (temperature, concentration of dye solutions, light source type, etc.).

The detection of gases and vapors of combustible organic substances [10,11] is one of the currently relevant areas of application of photocatalytic materials. In certain studies, photocatalytic detection of combustible gases was based on the exothermic reaction of their oxidation by ROSs generated by the photocatalyst under the influence of light. Composites containing noble metals (Pd [12,13], Pt [14]) were used as photocatalytic materials in detectors in these studies. This hinders the practical application of devices of this kind.

A technique for optical detection of combustible gases with the use of a photocatalyst of the $SnO-SnO_2-Fe_2O_3$ system developed in [15] was detailed in [10]. The efficiency of photocatalytic gas detection is largely determined by the properties of the photocatalyst used (spectral sensitivity range and ROS photogeneration capacity). Therefore, optimization of the chemical composition and structure of a photocatalyst is relevant for the development of optical

Table 1. Weighed quantities of initial components

Sample	$Zn(NO_3)_2$, g	$SnCl_2$, g	$Fe(NO_3)_3$, g	$AgNO_3$, g	PVP, g
ZnSnFe	2.5000	0.1065	0.0679	—	—
ZnSnFe(PVP)	2.5000	0.1065	0.0679	—	2.5000
ZnSnFeAg(PVP)	2.5000	0.1065	0.0679	0.0239	2.5000

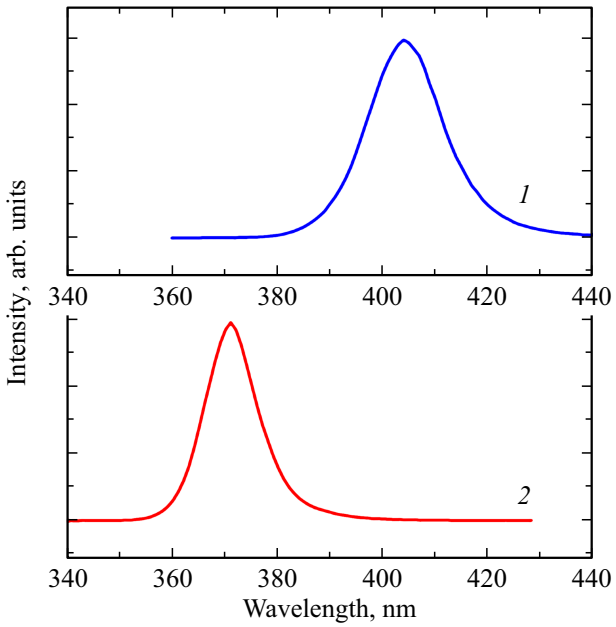

Figure 1. Emission spectra of LEDs used in the study: *1* — blue LED ($\lambda_{max} = 405$ nm); *2* — LED emitting in the near UV part of the spectrum ($\lambda_{max} = 375$ nm).

sensors of flammable organic compounds. The aim of the present study was to optimize the chemical composition and structure of a photocatalyst to improve its adsorption and photocatalytic properties.

It is known that a small amount of silver added to zinc oxide-based materials enhances their capacity to generate ROSs under the influence of light [16] and facilitates their involvement in photocatalytic processes [17,18].

Optimization of photocatalytic processes includes both adjustment of the chemical composition, crystal structure, and morphology of a photocatalytic material and selection of an external radiation source that provides the most efficient excitation of the photocatalyst used. Therefore, a complex analysis was performed in the present study to optimize a photocatalytic material with the use of light sources with different spectral compositions of radiation.

Materials and methods

The polymer-salt method was used to synthesize photocatalysts [5,6,16]. Tin chloride; zinc, iron, and silver nitrates; and polyvinylpyrrolidone (PVP, $M_w = 25000$-35000) were used as the starting materials for photocatalyst synthesis. Weighed quantities of metal salts and PVP with a given ratio of the initial components (Table 1) were dissolved in 25 ml of distilled water and dried at a temperature of 70°C.

Table 2. Elemental composition of composites according to the EMPA data

Elemental composition, mol.%	Zn	Sn	Fe	Ag
ZnSnFe	92.82	4.77	2.41	—
ZnSnFe(PVP)	91.13	5.22	3.65	—
ZnSnFeAg(PVP)	95.59	2.06	1.46	0.89

The obtained polymer-salt composites were subjected to heat treatment at a temperature of 550°C for two hours in an air atmosphere. These temperature and time parameters of heat treatment ensure that metal nitrates and the organic polymer decompose and gaseous products are removed completely [15].

X-ray diffraction analysis was performed to study the crystal structure of materials. A Rigaku SmartLAB 3 diffractometer (CuKα, 40 kV, 44 mA) was used in these experiments.

Diffuse reflectance spectra were measured with a Perkin Elmer 900 UV/VIS/NIR spectrophotometer. Photoluminescence spectra of the studied materials were measured using a Perkin Elmer LS-50B spectrofluorimeter within the 250–650 nm spectral range.

The morphology and elemental composition of the obtained composites were examined with a TescanVega 3 SBH scanning electron microscope (SEM) fitted with an Oxford INCA x-act electron microprobe analysis (EMPA) attachment.

The following light sources were used in photocatalytic experiments: an LED emitting in the near UV part of the spectrum ($\lambda_{max} = 375$ nm), an HPR40E LED emitting blue light ($\lambda_{max} = 405$ nm), and a DRT-250 high-pressure mercury lamp ($\lambda_{max} = 254$ nm in UV). Figure 1 shows the emission spectra of the LEDs used. The emission spectrum of the mercury lamp was presented in [19].

The Chicago Sky Blue (CSB, Sigma Aldrich) diazo dye, which was used in [5,6,19] to evaluate the photocatalytic activity of materials, served as a model organic pollutant component. A solution of this dye (0.01 g/l) was introduced into a quartz cell 3 ml in volume. A 0.0045 g sample of the nanocomposite secured to a flat glass substrate with double-sided tape was then introduced into this cell.

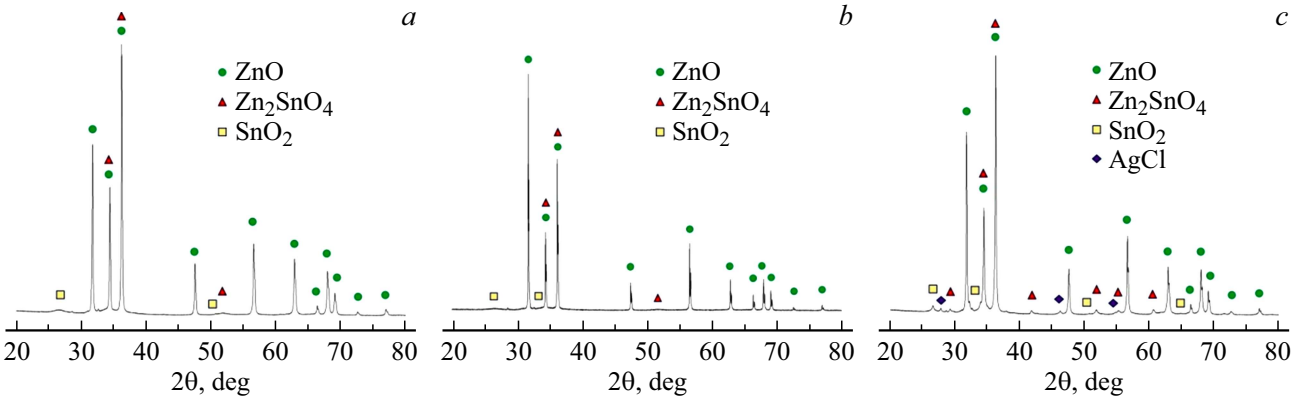

Figure 2. Diffraction patterns for ZnSnFe (*a*), ZnSnFe(PVP) (*b*), and ZnSnFeAg(PVP) (*c*) samples.

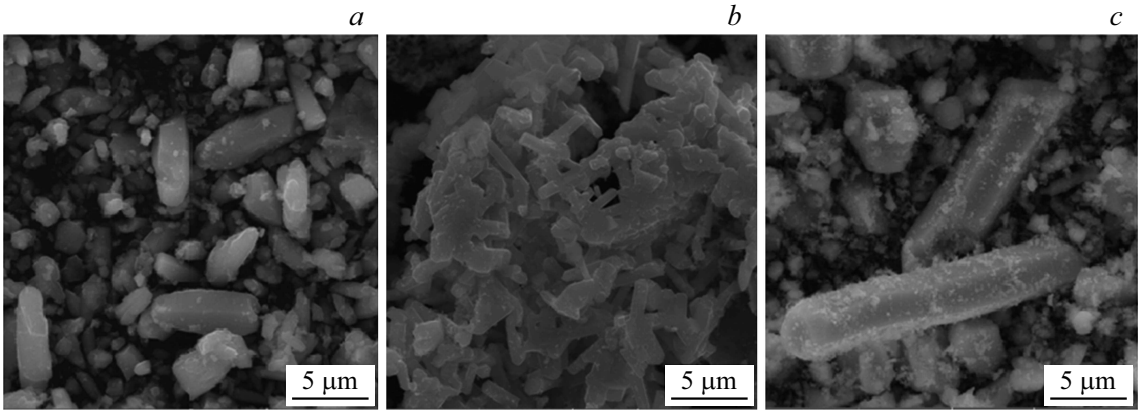

Figure 3. Electron microscopic images of ZnSnFe (*a*), ZnSnFe(PVP) (*b*), and ZnSnFeAg(PVP) (*c*) nanocomposites.

The light source was positioned at a distance of 7 cm from the cell with the dye and the photocatalyst in experiments on photocatalytic decomposition.

The concentration of the dye in solutions was determined in experiments on its adsorption and photocatalytic decomposition using a Perkin Elmer Lambda 650 UV/VIS spectrophotometer.

Results and discussion

Figure 2 shows the X-ray diffraction patterns of the obtained powders. It is evident that the materials contain zinc oxide crystals, tetragonal SnO_2 crystals, and Zn_2SnO_4 spinel. It should be noted that these components of synthesized composites have fine photocatalytic properties [5,6,11,20–24]. The AgCl phase is present in the sample synthesized with the addition of silver. The EMPA data for samples are listed in Table 2.

Figure 3 shows the electron microscopic images of powdered nanocomposites. It can be seen that the composites contain aggregates of micrometer-sized nanoparticles and smaller particles. A comparison of Figs. 3, *a* and 3, *b* reveals that PVP added to the initial solution facilitates the formation of a more disperse photocatalyst structure.

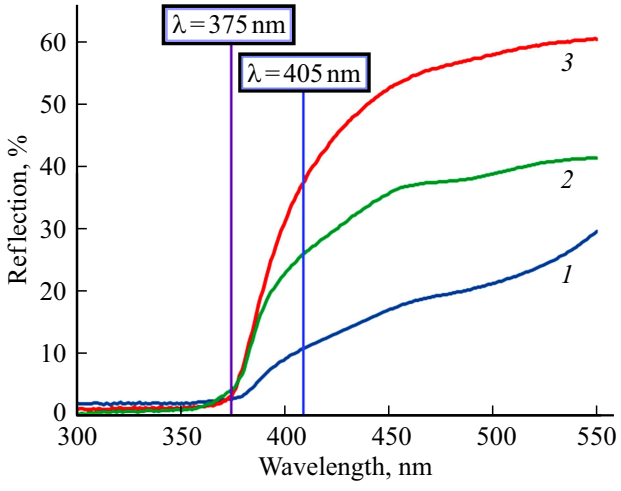

Figure 4. Diffuse reflectance spectra of ZnSnFe (*1*), ZnSnFe(PVP) (*2*), and ZnSnFeAg(PVP) (*3*) composites.

The diffuse reflectance spectra of nanocomposites are shown in Fig. 4. It is evident that the transparency cutoff of all materials is 375 nm (3.31 eV). This value is determined by the high concentration of zinc oxide with a band gap of

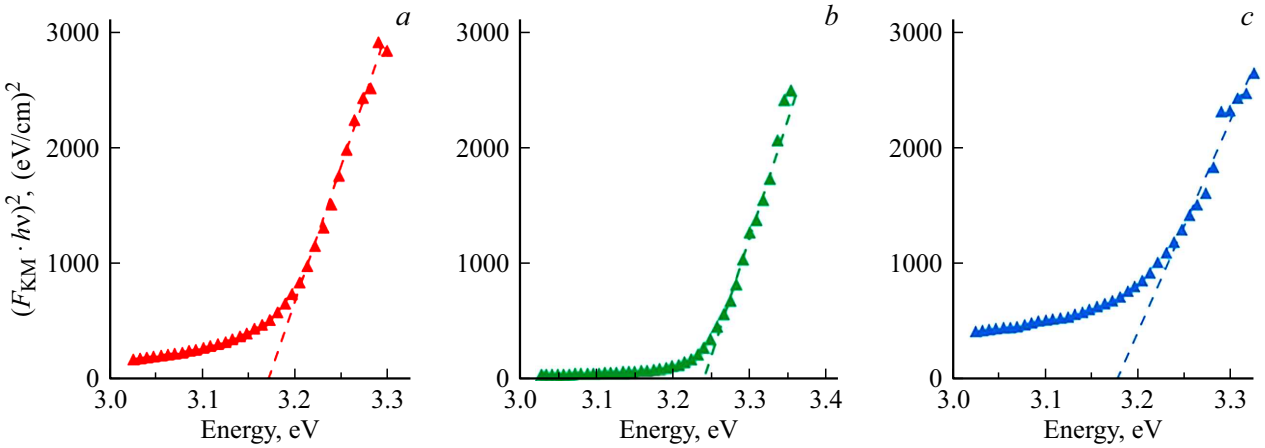

Figure 5. Dependences $(F_{KM}h\nu)^2 = f(h\nu)$ for ZnSnFe (*a*), ZnSnFe(PVP) (*b*), and ZnSnFeAg(PVP) (*c*) composites.

3.27 eV [25] in them. It may be noted that the introduction of relatively small amounts of silver into the composition enhances significantly the reflection of light in the visible part of the spectrum.

The reflectance spectra of composites 1 and 2 (curves *1* and *2* in Fig. 4) feature slight inflections at ~ 500–520 nm (2.38–2.48 eV), which may be indicative of light absorption in this range.

The obtained diffuse reflectance spectra of the examined materials were used to estimate the band gap with Kubelka–Munk function F_{KM}:

$$F_{KM} = \frac{(1-R^2)}{2R}, \qquad (1)$$

where R is the diffuse reflectance of a material measured relative to a perfectly white body. Band gap E_g in the obtained composites was estimated based on the calculated FKM values with the use of the Tauc equation [26]:

$$(F_{KM}h\nu)^2 = A(h\nu - E_g), \qquad (2)$$

where $h\nu$ is the photon energy, E_g is the band gap, and A is a constant. $(F_{KM}h\nu)^2 = f(h\nu)$ plots were used to evaluate E_g of the composites.

Figure 5 shows the $(F_{KM}h\nu)^2 = f(h\nu)$ dependences for the obtained composites. The E_g values for all materials were 3.17–3.24 eV. Thus, they were only slightly smaller than the band gap of ZnO (3.27 eV [25]). and close to the values of E_g determined earlier for the ZnO–SnO_2 (3.15–3.19 eV [27]) and ZnO–Fe_2O_3 (3.15 eV [28]) composites.

It is known that structural defects producing electron levels in the band gap of an oxide semiconductor may exert a significant influence on its photocatalytic properties [21]. Figure 6 shows the photoluminescence spectra of the ZnSnFe(PVP) composite at different excitation wavelengths.

The exciton luminescence band of ZnO found in the 390–395 nm region is observed under UV irradiation. Emission peaks with maxima at 415, 440, and 455 nm, which are attributed to structural defects of zinc oxide [29,30], emerge in the visible part of the spectrum. When the composite is irradiated with blue light, emission peaks are observed in the luminescence spectrum in different parts of the visible range (curve *3* in Fig. 6). Emission bands within the 525–575 nm spectral interval suggest the presence of oxygen vacancies in the structure of ZnO crystals [31]. It should be noted that the intensity ratio of bands corresponding to oxygen vacancies for the ZnSnFe(PVP) sample was lower than the one for the SnO–SnO_2–Fe_2O_3 composite with a similar composition, which was examined earlier in [15]. This difference may be attributed to the fact that iron chloride ($FeCl_3$) was the precursor in polymer-salt synthesis in our previous experiments [15], while $Fe(NO_3)_3$ was chosen in the present study. Nitrate has a greater oxidizing capacity than chloride and, when heated, may itself serve as a source of oxygen. This is the likely reason for the observed reduction in intensity of lines in the red part of the spectrum (relative to the spectrum of a similar composite in [15]) associated with a reduction in the number of oxygen vacancies. Thus, it can be concluded that the nanocomposite has structural defects that may affect its photocatalytic properties.

Figure 7, *a* presents the kinetic dependences of adsorption of the CSB dye on the surface of photocatalysts. It is evident that the photocatalysts with added PVP (curves *2* and *3*) have a higher adsorption activity than the sample synthesized by thermal decomposition of metal salts (curve *1*).

It is well known that the kinetics of adsorption of dyes on the surface of solids is often characterized by a pseudo-first-order equation of the following form [8,32]:

$$\frac{dq_t}{dt} = k_f(q_e - q_t), \qquad (3)$$

where q_t (mg/g) is the amount of dye adsorbed by 1 g of the sorbent at time point t; q_e is the equilibrium adsorption capacity of the sorbent; k_f (min^{-1}) is the adsorption rate constant; and t is the adsorption duration (min).

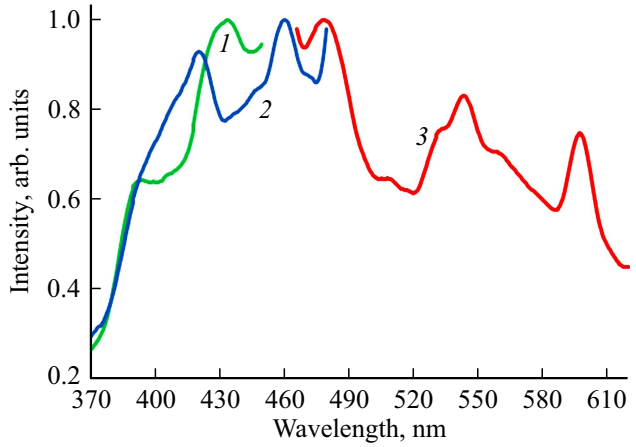

Figure 6. Photoluminescence spectra of the ZnSnFe(PVP) nanocomposite. Luminescence excitation wavelength: 239 (*1*), 256 (*2*), 400 nm (*3*).

Figure 7, *b* presents the $\ln(q_e - q_t) = f(t)$ dependences plotted based on the experimental data on adsorption of the dye on the surface of composites. It is evident that the experimental data agree closely with the linear dependences ($R^2 > 0.9$).

The pseudo-second-order kinetic equation is also used often to characterize the kinetics of adsorption of organic substances on the surface of photocatalysts [23,33] and may be presented in the following integral form:

$$\frac{t}{q_t} = \frac{1}{k_2 q_e^2} + \frac{t}{q_e}, \qquad (4)$$

where k_2 is the adsorption rate constant. Figure 7, *c* presents dependences $t/qt = f(t)$ of CSB adsorption on the surface of composites. It can be seen that the dependences are linear and that the pseudo-second-order kinetic equation provides a satisfactory fit to experimental data.

The kinetic dependences of photocatalytic decomposition of the dye in solutions under the influence of radiation from various sources are shown in Fig. 8.

A pseudo-first-order kinetic equation is often used to characterize the kinetics of photocatalytic decomposition of organic dyes in solutions [6,8,9,22,34]. Its integral form for dilute dye solutions ($C \ll 1$ mmole) is

$$C = C_0 e^{-kt}, \qquad (5)$$

where C_0 and C are the initial and current concentrations of a dye in a solution; k is the pseudo-first order rate constant of photocatalytic decomposition, min^{-1}; and t is time, min.

It can be seen from Fig. 8 that Eq. (5) provides a satisfactory fit ($R^2 > 0.9$) to all experimental data. A comparison of the kinetic dependences corresponding to different radiation sources reveals that the rate of photodecomposition of the dye reaches its maximum under the influence of mercury lamp radiation and decreases when UV and blue LEDs are used. The results of a comparative analysis of the emission spectra of LEDs (Fig. 1) and the diffuse reflectance spectra of the composites (Fig. 4) suggest that the observed significant reduction in the rate of photocatalytic decomposition of the dye is largely attributable to reduced absorption of blue ($\lambda_{\max} = 405$ nm) LED radiation by the composites.

At the same time, the data in Fig. 8, *c* indicate that visible radiation is suitable for decomposition of organic dyes with the use of the synthesized composites. Specifically, $\sim 40\%$ of dye molecules decompose within 40 min when the ZnSnFeAg(PVP) and ZnSnFe(PVP) composites are used.

A comparison of the kinetic dependences of adsorption of the dye on the surface of composites (Fig. 7, *a*) and its photocatalytic decomposition under the influence of UV radiation (Fig. 8, *a, b*) reveals that the rate of photocatalysis is significantly higher than the rate of dye adsorption. This effect has already been observed in [6,8,35] and attributed to the fact that both CSB molecules adsorbed on the surface and molecules in solution are subjected to the influence of ROSs released by the photocatalyst.

It follows from the data in Fig. 8 that the highest rate of dye decomposition is achieved when the ZnSnFeAg(PVP) composite is used as a photocatalyst. Thus, it can be concluded that the addition of small amounts of silver to $SnO-SnO_2-Fe_2O_3$ composites has a beneficial effect on their photocatalytic properties. It is also evident that the introduction of PVP into the composition of initial components helps improve the photocatalytic characteristics of materials.

Table 3 lists the data on rate constants of photocatalytic decomposition of the dye under the influence of mercury lamp radiation in the presence of various photocatalysts. Comparing the results of the present study with literature data, one finds that optimization of the chemical composition ensures the formation of a material with fine photocatalytic properties.

Conclusion

The photocatalytic properties of composites of the $SnO-SnO_2-Fe_2O_3$ system were enhanced after optimization of their chemical composition and structure achieved by introducing small amounts of silver into the material. The obtained composites consist of hexagonal ZnO nanocrystals, tetragonal SnO_2 crystals, and Zn_2SnO_4 spinel. The kinetic dependences of adsorption of the organic Chicago Sky Blue diazo dye from solutions on the surface of composites are characterized well by kinetic equations of both pseudo-first and pseudo-second order. The kinetics of photocatalytic decomposition of the dye in solutions under the influence of both UV and visible light is characterized well by a first-order kinetic equation. A comparison of the kinetic dependences of adsorption of the organic Chicago Sky Blue dye from solution onto the surface of composites and its photocatalytic decomposition revealed that the interaction of organic molecules with reactive oxygen species generated

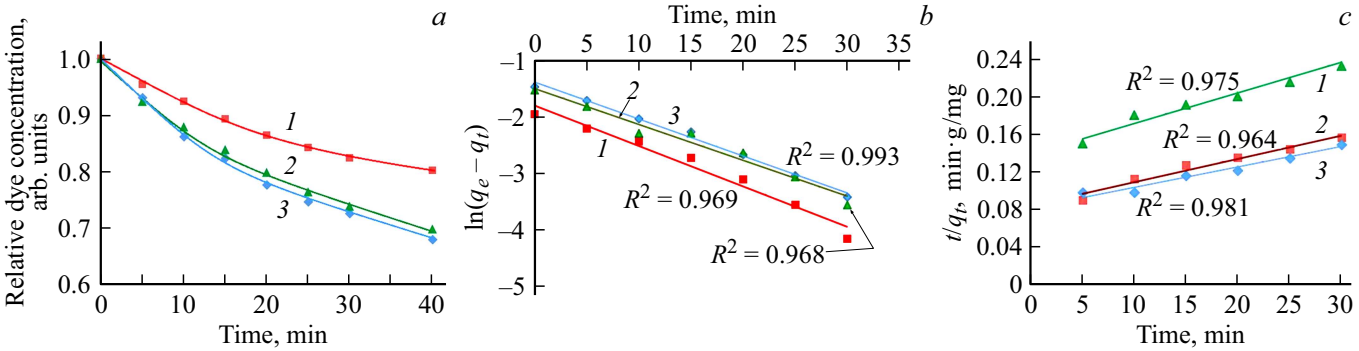

Figure 7. Kinetic dependences of CSB dye adsorption on the surface of photocatalysts (a), $\ln(q_e - q_t) = f(t)$ dependences (b), and $t/q_t = f(t)$ dependences (c) for ZnSnFe (*1*), ZnSnFe(PVP) (*2*), and ZnSnFeAg(PVP) (*3*) nanocomposites.

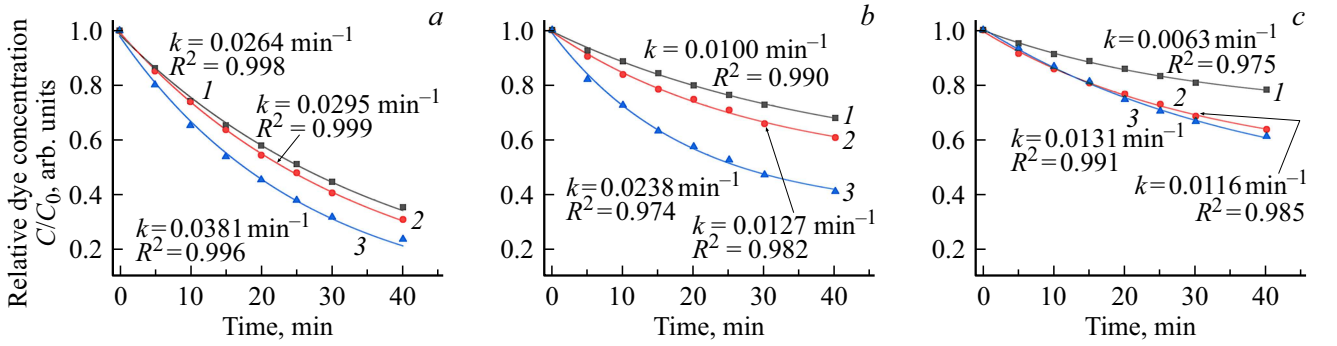

Figure 8. Photocatalytic decomposition curves of the CSB dye in the presence of ZnSnFe (*1*), ZnSnFe(PVP) (*2*), and ZnSnFeAg(PVP) (*3*) photocatalysts under the influence of mercury lamp radiation (a), UV diode emission with $\lambda_{max} = 375$ nm (b), and blue diode emission with $\lambda_{max} = 405$ nm (c).

Table 3. Rate constants of photocatalytic decomposition k of the CSB dye under the influence of mercury lamp radiation in the presence of various photocatalysts

№	Material of photocatalytic decomposition k, min^{-1}	Rate constant	Reference
1	Granular powder of ZnO	0.025	[6]
2	Porous powder of ZnO	0.042	[6]
3	Powder of ZnO 80.16 mol.% + $ZnAl_2O_4$ 19.83 mol.% + CuO 0.04 mol.%	0.021	[35]
4	Powder of ZnO 20.81 mol.% + $ZnAl_2O_4$ 79.18 mol.% + CuO 0.01 mol.%	0.005	[35]
5	ZnO „nanoflowers“	0.032	[36]
6	ZnSnFe	0.026	Experiment
7	ZnSnFe(PVP)	0.030	Experiment
8	ZnSnFeAg(PVP)	0.038	Experiment

by photocatalysts proceeds not only on the surface of the semiconductor composite, but also in the bulk solution. The maximum rate of photocatalytic decomposition of the dye (a decomposition rate constant of 0.038 min^{-1}) was observed in experiments with a composite of the SnO–SnO$_2$–Fe$_2$O$_3$ system modified with silver and synthesized from an initial mixture with polyvinylpyrrolidone added to it.

Funding

This study was supported in part (Evstropiev S.K.) by grant No. 20-19-00559 from the Russian Science Foundation.

References

[1] C.S. Turchi, D.F. Ollis. J. Catal., **122** (1), 178–192 (1990).
[2] Y. Li, W. Zhang, J. Niu, Y. Chen. ACS Nano, **6** (6), 5164–5173 (2012). DOI: 10.1021/nn300934k
[3] Y. Nosaka, A.Y. Nosaka. Chem. Rev., **117** (17), 11302–11336 (2017). DOI: 10.1021/acs.chemrev.7b00161
[4] Y. Jiang, S. Li, S. Wang, Y. Zhang, C. Long, J. Xie, X. Fan, W. Zhao, P. Xu, Y. Fan, C. Cui, Z. Tang. J. Am. Chem. Soc., **145** (4), 2698–2707 (2023). DOI:10.1021/jacs.2c13313
[5] L. Khomutinnikova, S. Evstropiev, I. Meshkovskii, I. Bagrov, V. Kiselev. Ceramics, **6** (2), 886–897 (2023). DOI: 10.3390/ceramics6020051
[6] M.A. Gavrilova, D.A. Gavrilova, S.K. Evstropiev, A.A. Shelemanov, I.V. Bagrov. Ceramics, **6** (3), 1667–1681 (2023). DOI:10.3390/ceramics6030103.K
[7] T. Wang, B. Tian, B. Han, D. Ma, M. Sun, A. Hanif, D. Xia, J. Shang. Energy & Environ. Mater., **5**, 711–730 (2022). DOI: 10.1002/eem2.12229
[8] A.S. Saratovskii, D.V. Bulyga, S.K. Evstrop'ev, T.V. Antropova. Glass Phys. Chem., **48** (1), 10–17 (2022). DOI: 10.1134/S1087659622010126.
[9] W. Zou, B. Gao, Y.S. Ok, L. Dong. Chemosphere, **218**, 845–859 (2019). DOI: 10.1016/j.chemosphere.2018.11.175
[10] L.L. Khomutinnikova, I.K. Meshkovskii, S.K. Evstropiev, M.Yu. Litvinov, E.P. Bykov, S.A. Plyastsov. Opt. Spectrosc., **131** (3), 399–404 (2023). DOI: 10/21883/OS.2023.03.55395.4525-23
[11] H. Li, S. Chu, Q. Ma, H. Li, Q. Che, J. Wang, G. Wang, P. Yang. ACS Appl. Mater. Interfaces, **11** (34), 31551–31561 (2019). DOI: 10.1021/acsami.9610410
[12] Y. Xia, J. Wang, L. Xu, X. Li, S. Huang. Sensors and Actuators B, **304**, 127334 (2020). DOI: 10.1016/j.anb.2019.127334
[13] Sh. Nasresfahani, M.N. Sheikhi, M. Tohidi, A. Zarifkar. Mater. Res. Bull., **89**, 161–169 (2017). DOI: 10.1016/j.materresbull.2017.01.032
[14] D. Zhang, H. Chang, Y. Sun, C. Jiang, Y. Yao, Y. Zhang. Sensors and Actuators B, **252**, 624–632 (2017). DOI: 10.1016/j.snb.2017.06.063
[15] L.L. Khomutinnikova, S.K. Evstropiev, D.P. Danilovich, I.K. Meshkovskii, D.V. Bulyga. J. Comp. Sci., **6**, 331 (2022). DOI: 10.3390/jcs6110331
[16] A.A. Shelemanov, S.K. Evstropiev, A.V. Karavaeva, N.V. Nikonorov, V.N. Vasilyev, Y.F. Podruhin, V.M. Kiselev. Mater. Chem. Phys., **276**, 125204 (2022). DOI: 10.1016/j.matchemphys.2021.125204
[17] T.N. Ravishankar, K. Manjunatha, T. Ramakrishnappa, Dhanith Nagaraju, S. Sarakar, B.S. Anadakumar, G.T. Chandrappa, Viswanath Reddy, J. Dupont. Mater. Sci. Semicond. Process., **26**, 7–17 (2014). DOI: 10.1016/j.mssp.2014.03.027
[18] Z. Cheng, S. Zhao, L. Han. Nanoscale, **10**, 6892–6899 (2018). DOI: 10.1039/c7nr09683f
[19] S.K. Evstropiev, V.N. Vasilyev, N.V. Nikonorov, E.V. Kolobkova, N.A. Volkova, I.A. Boltenkov. Chem. Engin. Process.: Process Intens., **134**, 45–50 (2018). DOI: 10.1016/j.cep.2018.10.020
[20] E.D. Foletto, J.M. Simões, M.A. Mazutti, S.L. Jahn, E.I. Muller, L.S.F. Pereira, E.M. de Moraes Flores. Ceram. Int., **39** (4), 4569–4574 (2017). DOI: 10.1016/j.ceramint.2012.11.053
[21] S. Bhatia, N. Verma. Mater. Res. Bull., **95**, 468–476 (2017). DOI: 10.1016/j.materresbull.2017.08.019
[22] L. Zhu, M. Hong, G.W. Ho. Sci. Rep., **5**, 11609 (2015).
[23] M.C. Uribe-López, M.C. Hidalgo-López, R. López-González, D.M. Frías-Márquez, G. Núñez-Nogueira, D. Hernández-Castillo, M.A. Alvarez-Lemus. J. Photochem. Photobiol. Chem., **404**, 112866 (2021). DOI: 10.1016/j.jphotochem.2020.112866
[24] J. Wang, H. Li, S. Meng, L. Zhang, X. Fu, S. Chen. Appl. Catalysis B, **200**, 19–30 (2017). DOI: 10.1016/j.apcatb.06.070
[25] H. Vahdat Vasei, S.M. Masoudpanah. J. Mater. Res. Technol., **11**, 112–120 (2021).
[26] J. Tauc. Mater. Res. Bull., **3**, 37–46 (1968).
[27] A. Hamrouni, N. Moussa, F. Parrino, A. Di Paola, A. Houas, L. Palmisano. J. Molec. Catalysis A, **390**, 133–141 (2014). DOI: 10.1016/j.molcata.2014.03.018
[28] L. Da Trindade, G.Y. Hata, J.C. Souza, M.R.S. Soares, E.R. Leite, E.C. Pereira, E. Longo, T.M. Mazzo. J. Mater. Sci., **55**, 2923–2936 (2020). DOI: 10/1007/s10853-019-04135-x
[29] S. Vempati, J. Mitra, P. Dawson. Nanoscale Res. Lett., **7**, 470 (2012). DOI: 10.1186/1556-276X-7-470
[30] H. Zeng, G. Duan, Y. Li, S. Yang, X. Xu, W. Cai. Adv. Funct. Mater., **20** (4), 561–572 (2020). DOI: 10.1002/adfm.200901884
[31] D. Das, P. Mondal. RSC Adv., **4**, 35735–35743 (2014). DOI: 10.1039/C4RA06063F
[32] Y. Kuang, X. Zhang, S. Zhou. Water, **12** (2), 587 (2020). DOI: 10.3390/w12020587
[33] U.I. Gaya, A.H. Abdullah. J. Photochem. Photobiol. C, **9**, 1–12 (2008). DOI: 10.1016/j.jphotochemrev.2007.12.003
[34] V. Loddo, M. Bellardita, G. Camera-Roda, F. Parnino, L. Palmisano. *Heterogeneous Photocatalysis: A promising advanced oxidation process.* (Elsevier Inc., 2018), Ch. 1. DOI: 10.1016/B978-0-12-813549-5.00001-3
[35] A. Shelemanov, A. Tincu, S.K. Evstropiev, N. Nikonorov, V. Vasilyev. J. Compos. Sci., **7**, 263 (2023). DOI: 10.3390/jcs7070263
[36] A. Mohammad, K. Kapoor, S.M. Mobin. Chemistry Select, **1**, 3483 (2016). DOI: 10.1002/slct.201600476

Translated by D.Safin